PAPER Special Issue on Analytical and Simulation Methods for Electromagnetic Wave Problems

Optimum Design of Power Coupling between Two Dielectric Slab Waveguides by the Boundary-Element Method Based on Guided-Mode Extracted Integral Equations

Dao Ngoc CHIEN[†a)], *Student Member*, Kazuo TANAKA[†], *and* Masahiro TANAKA[†], *Regular Members*

SUMMARY We show examples of accurate computer-aided design of power coupling between two dielectric slab waveguides of finite length by using the boundary-element method (BEM) based on guided-mode extracted integral equations (GMEIE's). The integral equations derived in this paper can be solved by the conventional BEM. Various properties in numerical calculations of GMEIE's are examined. The reflection and coupling coefficients of the guided wave as well as the scattering power are calculated numerically for the case of incidence TM guided-mode. The presented results are checked by the energy conservation law and reciprocity theorem. The results show that it is possible to design an optimum coupling between two dielectric slab waveguides by using the BEM based on GMEIE's.

key words: *coupling, slab waveguide, boundary integral equations, boundary-element method*

1. Introduction

A proper coupling between two waveguides for light-energy transfer between them plays an important role in the area of millimeter-wave, submillimeter-wave, and optical systems.

Many researchers have worked to find accurate and efficient methods for the analysis of optical dielectric waveguide circuits of complicated configuration. So far, the coupling between a solid-state laser and a planar dielectric waveguide has been investigated [1], and the analyses of coupling of a laser diode to a multimode fiber have also studied [2]. The extensive investigation has been done on the power coupling between waveguides that are either both planar [3]–[7], both circular [8], [9], or one circular and one planar [10]. Furthermore, the problem of arbitrarily discontinuities in planar dielectric waveguides has been treated in detail [11]–[13]. However, most of problems under consideration in these papers have restricted to the systems with the symmetrical geometry and/or the refractive indices of all the waveguides media are almost close, i.e., the weak-guidance condition is valid and the refractive index contrast between two waveguides is low. In addition, when we apply these techniques to the analysis of optical waveguide circuits, we have to combine with mode-expansion techniques of open waveguide structures that require complicated calculations and are not easy to perform.

Nowadays, the waveguides with strong-guidance condition and asymmetrical structure are widely used. So, the technique that gives the accurate reflection and coupling coefficients as well as the scattering power for the problem of power coupling between two dielectric slab waveguides with arbitrarily profiles of the refractive index is of great interest.

So far, we have proposed the boundary integral equations (BIE's) that are called guided-mode extracted integral equations (GMEIE's) [14]–[17]. If we use GMEIE's, we can avoid using mode-expansion techniques for open waveguide structures and can solve GMEIE's numerically by the conventional BEM or the moment method (MM). Because it is possible to investigate optical waveguide discontinuity problems such as scattering by an isolated dielectric object of finite size by using GMEIE's, they are suitable for use with CAD of dielectric optical waveguide circuits. In this paper, we show examples of accurate CAD of dielectric waveguide coupling for the symmetrical and asymmetrical geometries, including the systems with the high refractive index contrast between two waveguides.

The numerical results are presented for the case of incidence TM guided-mode. The results are verified by using the energy conservation law and the reciprocity theorem.

2. Boundary Integral Equations

We first introduce two types of coupling whose geometries are shown in Figs. 1(a) and (b).

In Fig. 1(a) the geometry of a matching-plate (MP) coupling is defined. An abruptly ended single-mode slab waveguide A is coupled the other slab waveguide B by using a matching-plate. The parameters of waveg-

Manuscript received March 17, 2003.
Manuscript revised May 12, 2003.

[†]The authors are with the Department of Electronics and Computer Engineering, Gifu University, Gifu-shi, 501-1193 Japan.
a) E-mail: chien@tnk.info.gifu-u.ac.jp

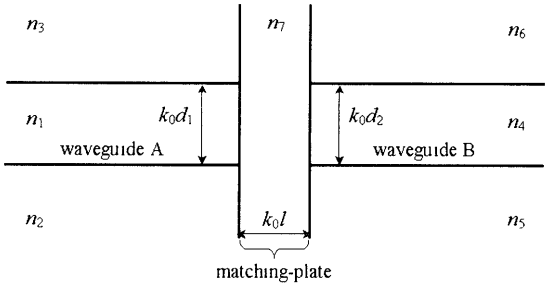

(a) Matching-plate coupling.

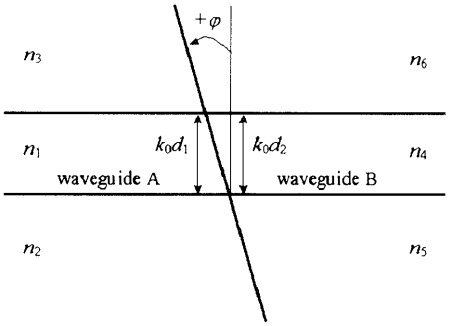

(b) Tilted-ends coupling.

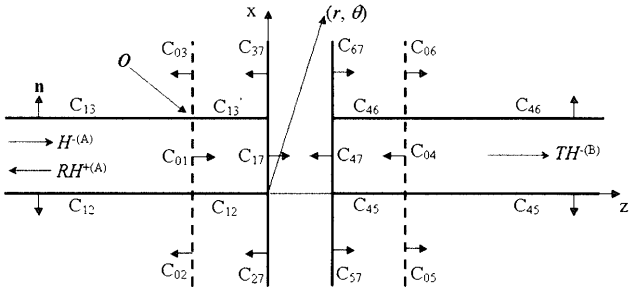

(c) Location of boundaries.

Fig. 1 Geometry of the problem under consideration.

uides and matching-plate are designed as shown in Fig. 1(a), where k_0 denotes the free-space wave number, $k_0 = \omega/c$, with c being the velocity of light in a vacuum. It can be seen that the geometry of a tilted-ends (TES) coupling as shown in Fig. 1(b) is a special case of MP coupling.

In the systems as shown in Figs. 1(a) and (b), to achieve true-mode guidance, it is necessary that the refractive index of core region (n_{co}) be larger than that of substrate (n_{su}) and cladding (n_{cl}) regions. If $n_{su} = n_{cl}$, we name it a symmetrical system. In the case $n_{su} \neq n_{cl}$, the system is asymmetrical. In this paper, it would be chosen: $n_{co} > n_{su} \geq n_{cl}$, i.e., $n_1 > n_2 \geq n_3$ and $n_4 > n_5 \geq n_6$.

If we assume that an incidence guided-mode from the waveguide A is directed toward the ended surfaces, we need to determine power of reflected guided-mode in waveguide A, power of transmitted guided-mode in waveguide B, and scattered power excited by the ended surfaces.

In the following analysis, a harmonic time dependence $\exp(+j\omega t)$ is assumed for the field quantities and is suppressed throughout the analysis. The whole space is assumed to be magnetically homogenous with a permeability $\mu = \mu_0$ of a vacuum. Since the two slab waveguides are assumed to be infinite extended in the y-direction, all field quantities are independent of y (i.e. $\partial/\partial y \equiv 0$).

In order to generate GMEIE's, we assume that a dominant TM guided-mode is incident from waveguide A directing toward the ended surfaces. The locations of the actual boundaries (solid lines) and virtual boundaries (dashed lines) are shown in Fig. 1(c). Let us note that the part from virtual boundaries to ended surfaces of longitudinal boundaries is specified by comma on the superscript. We consider the 2D Helmholtz equation, which is derived from Maxwell's equations. The Cartesian coordinate is used. We first consider the case in which the observation point $\mathbf{x}$ approaches the boundaries $C = C_{12} + C'_{12} + C_{17} + C'_{13} + C_{13}$ from inside of the waveguide A. The 2D Helmholtz equation is given by

$$\nabla^2 H_y(\mathbf{x}) + n_1^2 k_0^2 H_y(\mathbf{x}) = 0, \tag{1}$$

where $H_y(\mathbf{x})$ is the y-component of the magnetic field. The free-space Green's function $G_1(\mathbf{x}|\mathbf{x}')$ associated with Helmholtz Eq. (1) can be written as

$$\nabla^2 G_1(\mathbf{x}|\mathbf{x}') + n_1^2 k_0^2 G_1(\mathbf{x}|\mathbf{x}') = -\delta(\mathbf{x}|\mathbf{x}'), \tag{2}$$

where

$$G_1(\mathbf{x}|\mathbf{x}') = -\frac{j}{4} H_0^{(2)}(n_1 k_0 |\mathbf{x} - \mathbf{x}'|) \tag{3}$$

and $H_0^{(2)}(\mathbf{x})$ denotes the zero-order Hankel function of the second kind. The conventional BIE can be derived from Eqs. (1) and (2) as follows:

$$\frac{1}{2} H_y(\mathbf{x}) = \int_C \left[G_1(\mathbf{x}|\mathbf{x}') \frac{\partial H_y(\mathbf{x}')}{\partial n'} - H_y(\mathbf{x}') \frac{\partial G_1(\mathbf{x}|\mathbf{x}')}{\partial n'} \right] dl', \tag{4}$$

where the notation $\partial/\partial n'$ denotes the derivative with respect to the unit normal vector $\mathbf{n}$ to C as shown in Fig. 1(c). Since the magnetic field $H_y(\mathbf{x})$ includes the guided-mode fields and the boundaries $C_{12} + C_{13}$ is infinite length, $H_y(\mathbf{x})$ and $\partial H_y(\mathbf{x})/\partial n'$ on the boundaries are represented in infinite terms of a basic function when we try to apply the BEM or the MM to Eq. (4).

To subtract the guided-mode fields from the total magnetic field, we consider what kinds of field are included in the total magnetic field on the infinite-length boundaries $C_{12} + C_{13}$. Because the total magnetic field $H_y(\mathbf{x})$ on boundaries $C_{12} + C_{13}$ includes the incidence and reflected guided-mode fields, we consider that the total magnetic field can be decomposed as follows:

$$H_y(\mathbf{x}) = H_y^C(\mathbf{x}) + RH_y^{+(1)}(\mathbf{x}) + H_y^{-(1)} \quad (\mathbf{x} \text{ on } C_{12} + C_{13}), \tag{5}$$

where R indicates the reflection coefficient and $H_y^{\pm}(\mathbf{x})$ represent the reflected $(+)$ and incidence $(-)$ guided-mode fields, respectively. Since $H_y^C(\mathbf{x})$ represents the magnetic field that results from subtracting the guided-mode fields from the total field, $H_y^C(\mathbf{x})$ will vanish at points far away from the ended surfaces on boundaries $C_{12} + C_{13}$. The field $H_y^C(\mathbf{x})$ is called disturbed field [14]–[17].

The total magnetic field on the boundaries $C'_{12} + C_{17} + C'_{13}$, which are finite length, is also denoted by $H_y^C(\mathbf{x})$, i.e.,

$$H_y(\mathbf{x}) = H_y^C(\mathbf{x}) \quad (\mathbf{x} \text{ on } C'_{12} + C_{17} + C'_{13}). \tag{6}$$

Substituting Eqs. (5) and (6) into Eq. (4), we can derive the following equation:

$$\frac{1}{2}H_y^C(\mathbf{x}) = \int_C \left[G_1(\mathbf{x}|\mathbf{x}')\frac{\partial H_y^C(\mathbf{x}')}{\partial n'} - H_y^C(\mathbf{x}')\frac{\partial G_1(\mathbf{x}|\mathbf{x}')}{\partial n'}\right] dl' - RU_1^{+(A)}(\mathbf{x}) - U_1^{-(A)}(\mathbf{x}), \tag{7}$$

where

$$U_1^{\pm(A)}(\mathbf{x}) = \int_{C_{01}} \left[G_1(\mathbf{x}|\mathbf{x}')\frac{\partial H_y^{\pm(1)}(\mathbf{x}')}{\partial n'} - H_y^{\pm(1)}(\mathbf{x}')\frac{\partial G_1(\mathbf{x}|\mathbf{x}')}{\partial n'}\right] dl'. \tag{8}$$

In Eq. (7) the boundary integrals of guided-mode waves $H_y^{\pm(1)}(\mathbf{x})$ along the semi-infinite longitudinal boundaries $C_{12} + C_{13}$ can be reduced to that along finite virtual boundary C_{01}, as shown in Fig. 1(c). This relation can be obtained by applying Green's theorem to the guided-mode waves $H_y^{\pm(1)}(\mathbf{x})$ in the region surrounded by the boundary $C_{12} + C_{01} + C_{13}$.

In order to derive the expression of the reflection coefficient, R, in terms of $H_y^C(\mathbf{x})$ defined by Eqs. (5) and (6), we put the observation point $\mathbf{x}$ far away from the ended surfaces. Under this condition, it is possible to approximate Green's function by the asymptotic expression as

$$G_1(\mathbf{x}|\mathbf{x}') = A_1(r)g_1(\theta|\mathbf{x}'), \tag{9}$$

where

$$A_1(r) = -\frac{j}{4}\left(\frac{2j}{\pi n_1 k_0 r}\right)^{1/2}\exp(-jn_1k_0r), \tag{10}$$

$$g_1(\theta|\mathbf{x}') = \exp(jn_1k_0(z'\cos\theta + x'\sin\theta)). \tag{11}$$

Substituting Eq. (9) into Eq. (7), by using the straightforward mathematical procedures and let note that it is impossible for a reflected radiation field to exist at points in the waveguide A far away from ended surfaces, i.e.,

$$H_y^C(r, \pi) = 0 \quad (r \to \infty), \tag{12}$$

we can find that the reflection coefficient, R, can be expressed in term of the field $H_y^C(\mathbf{x})$ as

$$R = \left\{\int_C \left[g_1(\theta|\mathbf{x}')\frac{\partial H_y^C(\mathbf{x}')}{\partial n'} - H_y^C(\mathbf{x}')\frac{\partial g_1(\theta|\mathbf{x}')}{\partial n'}\right] dl' - u_1^{-(A)}(\theta)\right\} \Big/ u_1^{+(A)}(\theta), \tag{13}$$

where

$$u_1^{\pm(A)}(\theta) = \int_{C_{01}} \left[g_1(\theta|\mathbf{x}')\frac{\partial H_y^{\pm(1)}(\mathbf{x}')}{\partial n'} - H_y^{\pm(1)}(\mathbf{x}')\frac{\partial g_1(\theta|\mathbf{x}')}{\partial n'}\right] dl'. \tag{14}$$

Substitution of Eq. (13) into Eq. (7), we can obtain the GMEIE for the core region of waveguide A that is applicable to the BEM as follows:

$$\frac{1}{2}H_y^C(\mathbf{x}) = \int_C \left[P_1(\mathbf{x}|\mathbf{x}')\frac{\partial H_y^C(\mathbf{x}')}{\partial n'} - H_y^C(\mathbf{x}')\frac{\partial P_1(\mathbf{x}|\mathbf{x}')}{\partial n'}\right] dl' - S_1(\mathbf{x}), \tag{15}$$

where

$$P_1(\mathbf{x}|\mathbf{x}') = G_1(\mathbf{x}|\mathbf{x}') - g_1(\theta|\mathbf{x}')\frac{U_1^{+(A)}(\mathbf{x})}{u_1^{+(A)}(\theta)}, \tag{16}$$

$$S_1(\mathbf{x}) = U_1^{-(A)}(\mathbf{x}) - u_1^{-(A)}(\theta)\frac{U_1^{+(A)}(\mathbf{x})}{u_1^{+(A)}(\theta)}. \tag{17}$$

Since $H_y^C(\mathbf{x})$ will vanish at points far away from the ended surfaces, integral boundary $C_{12}+ C_{13}$, which have infinite length, can be regarded as finite in length in Eq. (15).

Next, to derive the expression of the transmission coefficient, T, we have also decomposed the total field on the boundary $C = C_{45} + C'_{45} + C_{47} + C'_{46} + C_{46}$ into the field components as follows:

$$H_y(\mathbf{x}) = TH_y^{-(4)}(\mathbf{x}) + H_y^C(\mathbf{x}), \quad (\mathbf{x} \text{ on } C_{45} + C_{46}) \tag{18}$$

$$H_y(\mathbf{x}) = H_y^C(\mathbf{x}). \ (\mathbf{x} \text{ on } C'_{45} + C_{47} + C'_{46}) \tag{19}$$

And by using the same procedure as that used in the above-derivation of Eq. (15) to the conventional BIE in the core region of slab waveguide B, we can obtain the expression of transmission coefficient, T, as follows:

$$T = \left\{\int_C \left[g_4(\theta|\mathbf{x}')\frac{\partial H_y^C(\mathbf{x}')}{\partial n'} - H_y^C(\mathbf{x}')\frac{\partial g_4(\theta|\mathbf{x}')}{\partial n'}\right] dl'\right\} \Big/ u_4^{-(B)}(\theta), \tag{20}$$

where

$$u_4^{-(B)}(\theta) = \int_{C_{04}} \left[g_4(\theta|\mathbf{x}') \frac{\partial H_y^{-(4)}(\mathbf{x}')}{\partial n'} - H_y^{-(4)}(\mathbf{x}') \frac{\partial g_4(\theta|\mathbf{x}')}{\partial n'} \right] dl'. \quad (21)$$

We can also obtain the GMEIE for the core region of waveguide B in terms of the field $H_y^C(\mathbf{x})$ as

$$\frac{1}{2} H_y^C(\mathbf{x}) = \int_C \left[P_4(\mathbf{x}|\mathbf{x}') \frac{\partial H_y^C(\mathbf{x}')}{\partial n'} - H_y^C(\mathbf{x}') \frac{\partial P_4(\mathbf{x}|\mathbf{x}')}{\partial n'} \right] dl', \quad (22)$$

with

$$P_4(\mathbf{x}|\mathbf{x}') = G_4(\mathbf{x}|\mathbf{x}') - g_4(\theta|\mathbf{x}') \frac{U_4^{-(B)}(\mathbf{x})}{u_4^{-(B)}(\theta)}, \quad (23)$$

and

$$U_4^{-(B)}(\mathbf{x}) = \int_{C_{04}} \left[G_4(\mathbf{x}|\mathbf{x}') \frac{\partial H_y^{-(4)}(\mathbf{x}')}{\partial n'} - H_y^{-(4)}(\mathbf{x}') \frac{\partial G_4(\mathbf{x}|\mathbf{x}')}{\partial n'} \right] dl'. \quad (24)$$

So far, we have considered the cases in which an observation point $\mathbf{x}$ approaches the boundaries from core region of slab waveguides. For the cases in which the observation point approaches the boundaries from substrate and cladding regions, also by using the same above-mentioned procedure that used in the derivation of Eqs. (15) and (22) to the conventional BIE's in the exterior regions, we can obtain the GMEIE's for the substrate and cladding regions of slab waveguides A and B in terms of the field $H_y^C(\mathbf{x})$ that are omitted here for saving space.

When the observation point $\mathbf{x}$ approaches the boundaries $C = C_{17} + C_{27} + C_{37} + C_{47} + C_{57} + C_{67}$ from matching-plate region, the well-known BIE for the total field $H_y^C(\mathbf{x})$ in the matching-plate region can be obtained easily.

The BIE's that derived in this paper are equations to be solved numerically for the problem shown in Figs. 1(a) and (b). They can be solved by use of the conventional BEM or MM with applying boundary conditions on the actual boundaries.

Once the fields on all the boundaries have been obtained, the reflection and transmission coefficients can be obtained with Eqs. (13) and (20). And fields at any point can also be calculated by boundary integral representations.

3. Radiation Field

The radiation field $H_y^{S(i)}(r,\ \theta)$ $(i = 2, 3, 4, 6)$ in the exterior regions can be expressed by use of an asymptotic form of Green's function in free-space with the corresponding refractive indices. Here, a typical example of the radiation field $H_y^{S(6)}(r,\ \theta)$ in the cladding region of waveguide B is obtained as follows.

As mentioned above, it is easy to derive the GMEIE for the cladding region of slab waveguide B as:

$$\frac{1}{2} H_y^C(\mathbf{x}) = -\int_{C_{46}+C'_{46}+C_{67}} \left[G_6(\mathbf{x}|\mathbf{x}') \frac{\partial H_y^C(\mathbf{x}')}{\partial n'} - H_y^C(\mathbf{x}') \frac{\partial G_6(\mathbf{x}|\mathbf{x}')}{\partial n'} \right] dl' - T U_6^{-(B)}(\mathbf{x}), \quad (25)$$

with

$$U_6^{-(B)}(\mathbf{x}) = \int_{C_{06}} \left[G_6(\mathbf{x}|\mathbf{x}') \frac{\partial H_y^{-(6)}(\mathbf{x}')}{\partial n'} - H_y^{-(6)}(\mathbf{x}') \frac{\partial G_6(\mathbf{x}|\mathbf{x}')}{\partial n'} \right] dl'. \quad (26)$$

By using the asymptotic form of Green's function in free-space with the refractive index n_6 in Eq. (25), the radiation field can be derived as:

$$H_y^{S(6)}(r,\theta) = -\frac{j}{4} \left(\frac{2j}{\pi n_6 k_0 r} \right)^{1/2} \exp(-j n_6 k_0 r) B_6(\theta), \quad (27)$$

where

$$B_6(\theta) = -\int_{C_{46}+C'_{46}+C_{67}} \left[g_6(\theta|\mathbf{x}') \frac{\partial H_y^C(\mathbf{x}')}{\partial n'} - H_y^C(\mathbf{x}') \frac{\partial g_6(\theta|\mathbf{x}')}{\partial n'} \right] dl' - T u_6^{-(B)}(\theta). \quad (28)$$

4. Computer-Aided Design

The integral equations were solved by use of the conventional BEM. The quadratic functions are used as basic functions, and delta functions are used as testing functions. The normalized discretization size for calculation was $k_0\ \delta = 0.2$. All semi-infinite boundaries are truncated at ten wavelengths length. The computation time was approximately 10 min to obtain one reflection and transmission coefficients. In this paper it would be chosen: $n_1 = 3.6$, $n_4 = 1.5$ to attain our aim that is optimum design of power coupling between two dielectric slab waveguides with the high refractive index contrast between them.

The most important problem in CAD always is accuracy of result. So, in order to verify the feasibility of the method in this paper, we used the energy conservation law and reciprocity theorem. In Table 1 the typical results of power-reflection coefficient Γ_R, power-transmission coefficient Γ_T, normalized scattering power Γ_S, and their total Γ_{TOTAL}, for the problem

Table 1 Power-reflection coefficient Γ_R, power-transmission coefficient Γ_T, normalized scattering power Γ_S, and their total Γ_{TOTAL} for the incidence from waveguide A (TM mode).

φ(°)	Γ_R	Γ_T	Γ_S	Γ_{TOTAL}
0	0 1172	0 4097	0 4727	0 9998
5	0 1659	0 4346	0 4000	1 0006
10	0 2198	0 4375	0 3433	1 0007
15	0 2633	0 4094	0 3281	1.0009
20	0 2451	0 3807	0 3740	0 9998
25	0 0003	0 1986	0 8017	1 0007

$k_0d_1 = k_0d_2 = 1$, $n_1 = 3\ 6$, $n_2 = n_3 = 3\ 24$, $n_4 = 1\ 5$, $n_5 = n_6 = 1\ 35$, $k_0l = 0$

Table 2 Verification of reciprocity between incident from waveguide A and incident from waveguide B.

φ(°)	Left-Hand Side of Eq (A4)	Right-Hand Side of Eq (A4)
0	-0 5618 +j2 8314	-0 5515 +j2 8435
5	-0 5505 +j2 9100	-0 5312 +j2 9125
10	-0 5801 +j2 8865	-0 5775 +j2 8756
15	-0 6261 +j2 7229	-0 6093 +j2 7255
20	-0 7318 +j2 5102	-0 7520 +j2 5100
25	-0 8606 +j1 6054	-0 8634 +j1 6332

$k_0d_1 = k_0d_2 = 1$, $n_1 = 3\ 6$, $n_2 = n_3 = 3\ 24$, $n_4 = 1\ 5$, $n_5 = n_6 = 1\ 35$, $k_0l = 0$

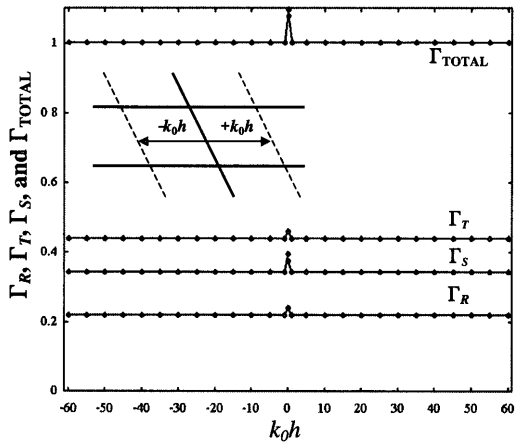

Fig. 2 The dependences of results on the location of virtual boundaries. The parameters are: $k_0d_1 = k_0d_2 = 1$; $n_1 = 3.6$, $n_2 = n_3 = 3.24$; $n_4 = 1.5$, $n_5 = n_6 = 1.35$; $k_0l = 0$, $\varphi = 10°$.

of TES coupling are shown. Where the parameters in calculations are: $k_0d_1 = k_0d_2 = 1$; $n_1 = 3.6$, $n_2 = n_3 = 3.24$; $n_4 = 1.5$, $n_5 = n_6 = 1.35$; $k_0l = 0$. We see that the results satisfy the energy conservation law within an accuracy of 0.1% well. In Table 2 the results of the reciprocity relation (A·4) (see Appendix) between the incidences from waveguide A and from waveguide B are presented for the same system as in Table 1. If the numerical results are fairly accurate, the second column that contains values of the left-hand side of Eq. (A·4) should coincide with the third column that contains values of the right-hand side of Eq. (A·4). We find that the numerical results satisfy the reciprocity relation fairly well in Table 2.

We have also explored the dependence of our results on the location of virtual boundaries in Fig. 2.

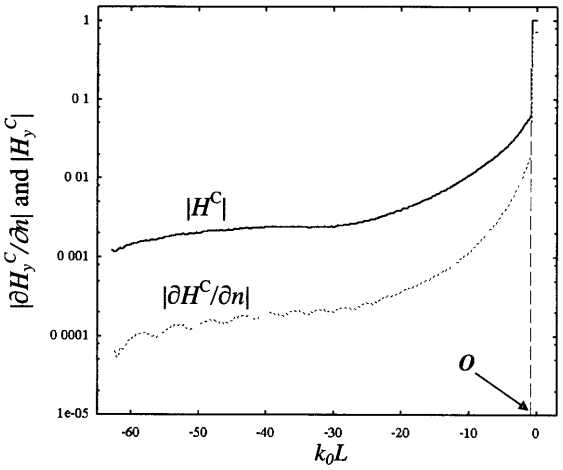

Fig. 3 Distribution of absolute values of the field $H_y^C(\mathbf{x})$ and its derivative $\partial H_y^C/\partial n$ along the boundary $C_{13} + C'_{13}$ of slab waveguide A. The abscissa is the normalized distance from the origin. The parameters are the same as in Table 1 with $\varphi = 5°$.

Here when the location of the virtual boundary $C_{01} + C_{02} + C_{03}$ is fixed, that of $C_{04} + C_{05} + C_{06}$ is moved from +0.001 to +60(9.55λ); and if that of $C_{01} + C_{02} + C_{03}$ is changed from −0.001 to −60 (9.55λ), then $C_{04} + C_{05} + C_{06}$ is fixed. The waveguides parameters are the same as in Table 1 with the tilted angle $\varphi = 10°$. It is seen that the results are independent of location of virtual boundaries, except the locations at ±0.001. This error is caused by the numerical method used, because when the virtual boundaries approach the ended surfaces, the coupling section approaches zero.

In order to show the validity of assumption (12), it is necessary to check field distributions in core region of waveguide A. If assumption (12) is correct, the field $H_y^C(\mathbf{x})$ must converge far from the ended surfaces. Figure 3 shows plots of these characteristics. The abscissa k_0L in Fig. 3 represents distance from the origin. The log-scale used for plots of $H_y^C(\mathbf{x})$ and $\partial H_y^C/\partial n'$. It is found that the disturbed field $H_y^C(\mathbf{x})$(left-hand side of dashed line) becomes enough small comparing with the total field $H_y^C(\mathbf{x})$(right-hand side of dashed line) to be regarded as vanished. In other words, assumption (12) is validated.

From the above-mentioned results, we can conclude that the numerical results in this paper are fairly accurate and the formulation used in this paper is mathematically correct.

5. Optimization of the Coupling Geometry

We show the examples of the CAD by the BEM based on GMEIE's: We consider the problem of finding optimum geometries that gives maximum transmission power between two-given dielectric slab waveguides as follows:
Symmetrical case with:

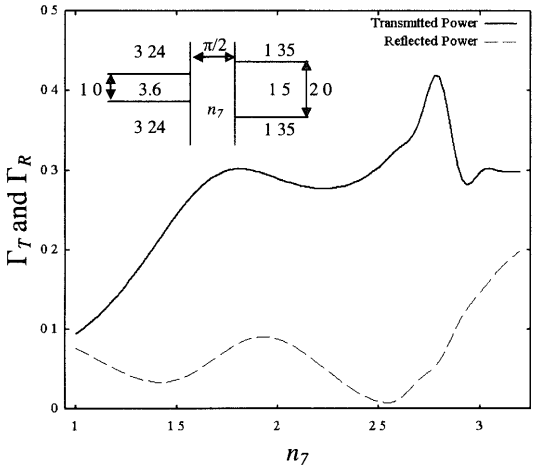

(a) Symmetrical.

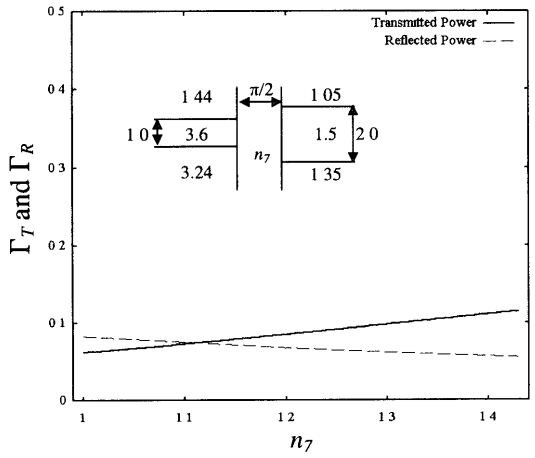

(b) Asymmetrical.

Fig. 4 Variation of Γ_R and Γ_T with the refractive index of the matching-plate n_7 for the case of (a) symmetrical and (b) asymmetrical structure. The optical thickness of matching-plate is: $k_0 l = \pi/2$.

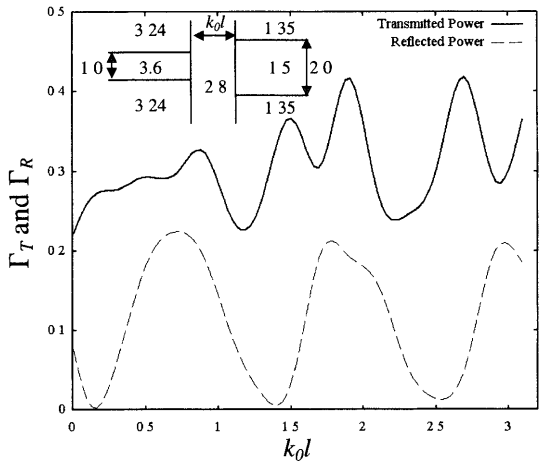

(a) Symmetrical.

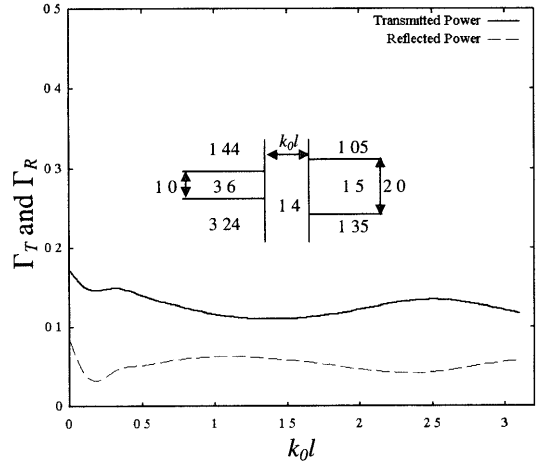

(b) Asymmetrical.

Fig. 5 Variation of Γ_R and Γ_T with the optical thickness of the matching-plate $k_0 l$ for the case of (a) symmetrical and (b) asymmetrical structure Where the refractive index of the matching-plates n_7 are given by: (a) 2.8 and (b) 1.4

Waveguide A:

$k_0 d_1 = 1,\ n_1 = 3.6,\ n_2 = n_3 = 3.24,$

Waveguide B:

$k_0 d_2 = 2,\ n_4 = 1.5,\ n_5 = n_6 = 1.35.$

Asymmetrical case with:

Waveguide A:

$k_0 d_1 = 1,\ n_1 = 3.6,\ n_2 = 3.24,\ n_3 = 1.44,$

Waveguide B:

$k_0 d_2 = 2,\ n_4 = 1.5,\ n_5 = 1.35,\ n_6 = 1.05.$

Let us start with the well-known fact that, for a film whose optical thickness has any of the values $\lambda/4$, $3\lambda/4$, $5\lambda/4$, ... the reflectivity is a maximum or a minimum according to whether the refractive index of the film is greater or smaller than the refractive index of the last medium [18]. We first use the MP coupling for connecting between the two above-given slab waveguides, whose numerical results are shown in Figs. 4 and 5. In these figures solid and dashed curves show power-transmission and power-reflection coefficients, results, respectively. Let us note that in Figs. 4(a) and (b) the ranges of horizontal axis are different because of the refractive index of the matching-plate must not satisfy the waveguide condition.

In Figs. 4(a) and (b) we fixed the optical thickness of the matching-plate at a quarter of wavelength, i.e., $k_0 l = \pi/2$. By changing the refractive index of matching-plate n_7 we searched for the optimum values and could find the optimum values for the both (a) symmetrical and (b) asymmetrical cases. From Fig. 4(a) it is found that it is possible to improve transmission characteristics of symmetrical structure from approximately $\Gamma_T = 0.22$ of the without matching-plate coupling to approximately $\Gamma_T = 0.42$ by using a matching-plate with optical thickness $k_0 l = \pi/2$ and refractive index $n_7 \approx 2.8$. On the contrary, from Fig. 4(b) it is seen that it is impossible to improve coupling efficiency of asymmetrical structure by using a matching-plate because of

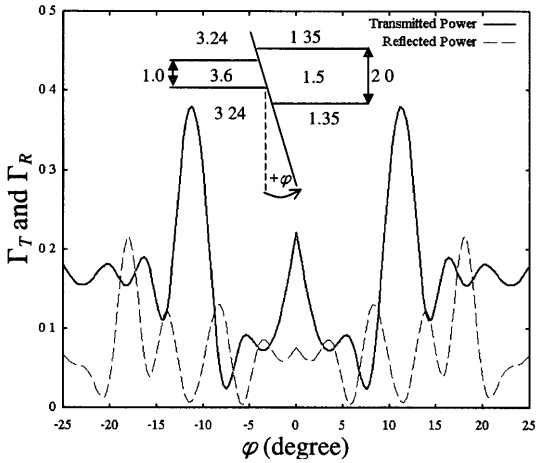

(a) Symmetrical.

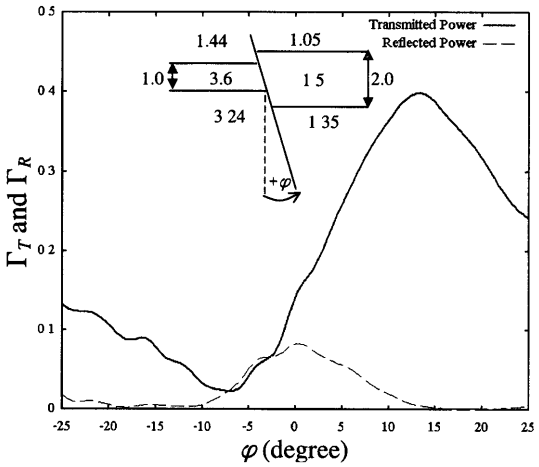

(b) Asymmetrical.

Fig. 6 Variation of Γ_R and Γ_T with the tilted angle φ for the case of (a) symmetrical and (b) asymmetrical structure.

the optimum approximately $\Gamma_T = 0.12$ is smaller than the approximately $\Gamma_T = 0.17$ for the case of coupling without matching-plate.

In Figs. 5(a) and (b) the refractive index of the matching-plates are given by 2.8 and 1.4 for the symmetrical and asymmetrical structures, respectively. By changing the optical thickness of matching-plate $k_0 l$, we also searched for the optimum values and could find those for the both (a) symmetrical and (b) asymmetrical cases. From Fig. 5(a) it is found that it is also possible to improve coupling efficiency of symmetrical structure to approximately $\Gamma_T = 0.42$ by using a matching-plate with refractive index $n_7 = 2.8$ and optical thickness $k_0 l \approx 1.9$ or 2.7. From Fig. 5(b) the remarks are the same as that for Fig. 4(b).

As we have investigated in detail [17], the power-transmission coefficient of a tilted-end dielectric slab waveguide increases following the increase of tilted angle. Based on above-mentioned idea we next consider the using of TES coupling for connection. We searched for the optimum values by changing the tilted angle φ.

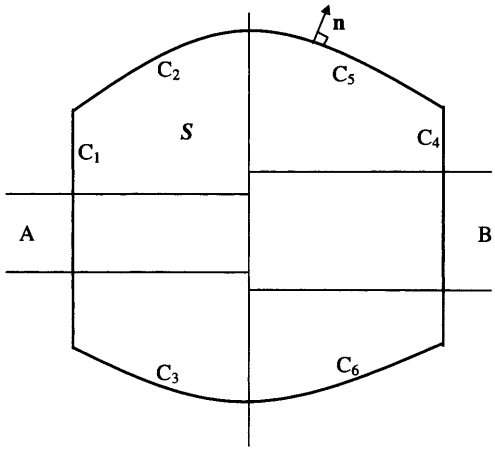

Fig. 7 Region S and boundaries C_i ($i = 1, 6$) used in the derivation of reciprocity relation.

We also found the optimum geometries for the both symmetrical and asymmetrical structures as shown in Figs. 6(a) and (b), respectively. In Fig. 6(a) we see that there are two angles $\varphi \approx \pm 12°$ that give maximum transmitted power, however, with the approximately $\Gamma_T = 0.39$ which is smaller than the approximately $\Gamma_T = 0.42$ as shown in Figs. 4(a) and 5(a). The results in Fig. 6(b) show the results of asymmetrical case. It is very nice, as expected, that the coupling coefficient can be improved from approximately $\Gamma_T = 0.17$ up to approximately $\Gamma_T = 0.40$ by using the TES coupling with the tilted angle $\varphi \approx +14°$.

From the above-presented examples, it has been found that we can obtain an accurate design of an optimum coupling geometry between two arbitrarily-profile dielectric slab waveguides by using a BEM based on GMEIE's. The numerical results show that the coupling characteristic between two symmetrical slab waveguides can be improved significantly by use of a matching-plate with the suitable chosen optical parameters. For coupling between two asymmetrical slab waveguides, the coupling characteristic can also be much improved by making a suitable tilted angle.

6. Conclusion

We showed examples of computer-aided design (CAD) of two-dimensional optical waveguide coupling by the BEM based on GMEIE's. From numerical examples it is shown that we can obtain an accurate CAD of an optimum coupling shape between two arbitrarily-profile dielectric optical waveguides.

The boundary integral equations derived in this paper can be solved by the conventional BEM for the waveguide discontinuity problems with finite-size which can be perfectly regarded as problems of scattering by an isolated dielectric object. It is possible to extend GMEIE's to multimode problems and three-dimensional problems. In the future we will apply this

method to the more complicated optical circuits such as asymmetrical T-junctions and asymmetrical Mach-Zehnder interferometry structures.

Acknowledgement

Dao Ngoc Chien acknowledges the Rotary Yoneyama Memorial Foundation, Inc. for their support of the Yoneyama Scholarship.

References

[1] G.A. Hockham and A.B. Sharpe, "Dielectric-waveguide discontinuities," Electron. Lett , vol 8, pp 230–231, May 1972.
[2] K. Kawano, H Miyazawa, and O Mitomi, "New calculations for coupling laser diode to multimode fiber," J Lightwave Technol , vol.LT-4, pp.368–374, May 1986.
[3] P. Gelin, M Petenzi, and J. Citerne, "New rigorous analysis of the step discontinuity in a slab dielectric waveguide," Electron. Lett., vol.15, pp.355–356, May 1979.
[4] T Takenaka and O Fukumitsu, "Accurate analysis of the abrupt discontinuity in a dielectric waveguide," Electron. Lett., vol 19, pp.806–807, July 1983
[5] K Uchida and K. Aoki, "Scattering of surface waves on transverse discontinuities in symmetrical three-layer dielectric waveguides," IEEE Trans Microw Theory Tech., vol.MTT-32, no.1, pp 11–19, Jan. 1984
[6] C.S. Rocha, "Scattering of surface waves at dielectric slab waveguide with axial ascending discontinuity," IEEE Trans. Magn , vol.34, no.5, pp 2720–2723, Sept 1998.
[7] G. Kweon and I. Park, "Splicing losses between dissimilar optical waveguides," J Lightwave Technol., vol.17, pp.690–703, April 1999.
[8] D Marcuse, "Loss analysis of single-mode fiber splices," Bell Syst. Tech J , vol.56, pp.703–718, May–June 1977.
[9] C N. Capsalis, N.K. Uzunoglu, and I.G. Tigelis, "Coupling between two abruptly terminated single-mode optical fibers," J. Opt. Soc Am. B, vol 5, pp.1624–1630, Aug. 1988.
[10] C.N Capsalis and N.K. Uzunoglu, "Coupling between an abruptly terminated optical fiber and a dielectric planar waveguide," IEEE Trans. Microw Theory Tech., vol.MTT-35, no.11, pp.1043–1051, Nov 1987.
[11] S. Chung and C H. Chen, "A partial variational approach for arbitrary discontinuities in planar dielectric waveguides," IEEE Trans Microw Theory Tech., vol 37, no.1, pp.208–214, Jan. 1989.
[12] K Hirayama and M. Koshiba, "Analysis of discontinuities in an open dielectric slab waveguide by combination of finite and boundary elements," IEEE Trans Microw. Theory Tech , vol.37, no.4, pp.761–767, April 1989.
[13] K Hirayama and M. Koshiba, "Numerical analysis of arbitrarily shaped discontinuities between planar dielectric waveguides with different thicknesses," IEEE Trans. Microw Theory Tech , vol.38, no 3, pp.260–264, March 1990.
[14] K Tanaka and M. Kojima, "New boundary integral equations for computer-aided design of dielectric waveguide circuits," J. Opt Soc. Am A, vol.6, pp 667–674, May 1989.
[15] K. Tanaka, M. Tanaka, H. Tashima, H. Ootera, and Y. Yoshino, "New integral equation method for CAD of open waveguide bends," Radio Sci., vol.28, pp.1219–1227, Nov. 1993.
[16] K Tanaka and M. Tanaka, "Computer-aided design of dielectric optical waveguide bends by the boundary-element method based on guided-mode extracted integral equations," J. Opt Soc. Am. A, vol.13, pp.1362–1368, July 1996.
[17] D.N. Chien, M. Tanaka, and K Tanaka, "Numerical simulation of an arbitrarily ended asymmetrical slab waveguide by guided-mode extracted integral equations," J Opt Soc. Am A, vol.19, pp.1649–1657, Aug 2002.
[18] M. Born and E. Wolf, Principles of Optics, 5th ed., Chap 1, Pergamon Press, New York, 1975,

Appendix: Reciprocity Relation

We start from the 2D reciprocity relation

$$\int_C \left(H_A \frac{\partial H_B}{\partial n} - H_B \frac{\partial H_A}{\partial n} \right) dl = 0, \quad (\mathrm{C} = \mathrm{C}_1 + \mathrm{C}_2 + \mathrm{C}_3 + \mathrm{C}_4 + \mathrm{C}_5 + \mathrm{C}_6), \qquad (\mathrm{A}\cdot 1)$$

where H_A and H_B denote the total fields due to the incident from waveguide A and waveguide B, respectively, and can be written as

$$H_A = \begin{cases} H_A^- + R_A H_A^+ + H_A^C & \text{on } \mathrm{C}_1 + \mathrm{C}_2 + \mathrm{C}_3 \\ T_A H_B^- + H_A^C & \text{on } C_4 + \mathrm{C}_5 + \mathrm{C}_6 \end{cases}, \qquad (\mathrm{A}\cdot 2)$$

$$H_B = \begin{cases} T_B H_A^+ + H_B^C & \text{on } \mathrm{C}_1 + \mathrm{C}_2 + \mathrm{C}_3 \\ H_B^+ + R_B H_B^- + H_B^C & \text{on } \mathrm{C}_4 + \mathrm{C}_5 + \mathrm{C}_6 \end{cases}, \qquad (\mathrm{A}\cdot 3)$$

where R_{ch} and T_{ch} $(ch = A, B)$ are reflection and transmission coefficients, respectively.

Substituting Eqs. (A·2) and (A·3) into Eq. (A·1), moving the boundary C to far from the origin, and concerning the condition that the radiation fields have to vanish in the directions of the waveguides, i.e., $\theta = 0$, π, we can obtain the compact reciprocity relation for the incident TM guided-mode as follow:

$$T_B \int_{\mathrm{C}_1} \left(H_1^- \frac{\partial H_1^+}{\partial n} - H_1^+ \frac{\partial H_1^-}{\partial n} \right) dl = T_A \int_{\mathrm{C}_4} \left(H_2^- \frac{\partial H_2^+}{\partial n} - H_2^+ \frac{\partial H_2^-}{\partial n} \right) dl. \qquad (\mathrm{A}\cdot 4)$$

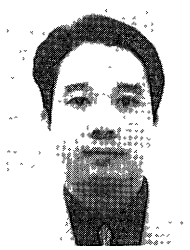

Dao Ngoc Chien received the B.E degree from the Department of Telecommunications Systems, Faculty of Electronics and Telecommunications, Hanoi University of Technology, Hanoi, VIETNAM in 1997 and there in the same year he became a Teaching Assistant. He received the M.S degree from the Department of Electronics and Computer Engineering, Gifu University, JAPAN in 2002, and is currently working towards the Ph D degree. His research since 1997 has been optical fiber communication systems and he is currently interested in the CAD of optical waveguide circuits. He is a student member of IEEE and OSA.

Kazuo Tanaka received the B.E., M.S., and Ph.D., degrees from the Department of Communications Engineering, Osaka University, Osaka, JAPAN in 1970, 1972 and 1975, respectively. In 1975, he became a Research Associate in the Department of Electrical Engineering at Gifu University He was an associate Professor in the Department of Electronics and Computer Engineering there in 1985 and in 1990 he was named Professor. His research since 1970 has been a general-relativistic electromagnetic theory and application, radiographic image processing and computational electromagnetic and he is currently interested in the CAD of integral optical circuits, near-field optical circuits and simulation of Anderson localization hypothesis of ball-lightning. He was a visiting Professor of University of Toronto, Canada in 1994. In 1987, he was awarded the Uchida Paper Award by the Japan Society of Medical Imaging and Information Science. He is now a chair of Technical Group of Electromagnetic Theory of IEICE in Japan.

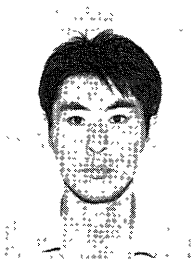

Masahiro Tanaka received the B.E. and M.S. degrees from the Department of Electrical and Computer Engineering, Gifu University, Gifu, JAPAN in 1992 and 1994, respectively. He received the Ph.D. degree from the Department of Communication Engineering, Osaka University, Osaka, JAPAN in 2002. He was a Research Associate at Tokoha-Gakuen Hamamatsu University from 1994 to 1996. He joined Gifu University as a research assistant in 1996. He was a visiting researcher at the Department of Electrical and Computer Engineering, The University of Arizona, USA from 1997 to 1998. His research interests are the CAD of optical waveguide circuits and near-field optical circuits.